

Porosity detection in CFRP using reflective terahertz imaging

YANDONG GONG*, JIANXIONG TANG, KAI PANG

School of Instrument Science and Optoelectronics Engineering, Beijing Information Science and Technology University, Beijing, 100192, PR China

Terahertz (THz) waves are potential safe and non-destructive inspection tool for industrial use. Reflective THz imaging using THz time-domain spectroscopy (THz-TDS) has been demonstrated as a fast, accurate, non-contact, and non-destructive inspection approach to evaluate the sub-surface layer porosity distribution of carbon fiber reinforced polymer (CFRP) materials used in aerospace. Our experiments show that the reflected THz amplitude and the time of flight (ToF) from THz imaging, can be used as parameters to evaluate porosity distributions. The volumetric average sensitivity of porosity tests based on amplitude imaging and ToF imaging reached ~3.5 % and ~2.5 %, respectively.

(Received March 7, 2022; accepted October 5, 2022)

Keywords: Terahertz, Porosity, Non-destructive inspection, Composite

1. Introduction

Carbon fiber reinforced polymer (CFRP) are widely used in many industrial sectors, including aerospace, due to their high strength, light weight, and stiffness. The main features that make CFRP so attractive are their strength-to-weight ratio and ability to be shaped into complex parts. However, the inherent porosity of these materials is a critical issue that determines the quality of fabricated parts. The strength of CFRP will be drastically reduced if its porosity exceeds 5% of its volume. Therefore, it is very important to inspect the porosity distribution of CFRP materials [1–3].

In this paper, pores are very small air voids (typically $\ll 0.1$ mm diameter) distributed in a material. Porosity is a measure of these air voids, and is given as the ratio of the volume of air voids to the total volume. Pores do not produce strong reflections, in contrast to delamination, but cause scattering; the measurement of porosity is based on the size and the density of pores within a defined area of interest. For laminate composites, porosity in the inner laminar bonding can lead to disbonding between the laminates, and pore cluster sites grow over time, typically lead to cracks over time.

Thermal imaging, ultrasonic imaging, and micro-computerized tomography (CT) scanning are porosity inspection methods commonly used in industry, and their typical detection sensitivity is poorer than 5% [2–4]. However, thermal and ultrasonic inspection share the disadvantage of poor image resolution that is insufficient to observe low levels of porosity, while CT uses radiative X-rays, which are ionizing and harmful. Thermal imaging is useful only when the pore region has grown to become a localized disbond or blister, or if the delamination sites are 3 mm or larger in diameter. To overcome all these disadvantages, an accurate, effective, and non-destructive

inspection (NDI) technique must be developed. In this paper, we report a safe and non-destructive terahertz (THz) imaging technology to detect porosity.

THz rays are in the electromagnetic (EM) band with a frequency range of 100 GHz–10THz, which is located between the microwave and IR bands. Neither microwave nor optical techniques can be directly applied in this band. In particular, THz radiation has several unique features: (1) Many polar molecules have specific THz spectroscopic fingerprints, (2) THz waves are safe and non-ionizing as the magnitude of their photon energy is $\sim 10^6$ times lower than that of X-rays, and (3) THz waves can penetrate paper, clothes, glass, polymers, ceramics, dry wood, and so forth, but they are reflected by metals and are strongly absorbed by water [5]. Thus, THz technology has attracted considerable interest for NDI applications in the industrial, security, and biomedical fields.

Recently, the importance of THz technology for checking the quality of aerospace composites has been recognized [6,7]. THz technology and instrumentation have provided new effective tools to inspect the defects and thicknesses of layers in CFRP. THz imaging typically has a spatial resolution of ~ 0.1 mm level, which is better than that of ultrasonic imaging. Ultrasound waves also require direct physical contact between the sensor and the object of interest as coupling from free space is not possible due to the high impedance mismatch [8]. This is not a problem for THz waves. Terahertz imaging has been used to detect composite delamination and impact damage in composites [9–11], while Kwang [12] used the transmission and reflectivity at orthogonal polarizations to differentiate delamination successfully. THz spectroscopy and imaging also have proved to be effective NDI tools for composite inspections, [12] with THz time domain spectroscopy (THz-TDS) being the most often used scheme.

Due to the characteristics of THz spectroscopy and imaging, they can be used for the non-contact and non-destructive porosity detection of composites [13,14]. In previous reports, the THz amplitude in the transmission setup has been used to detect porosity [15-17]. The detection sensitivity is close to 5%, although there is a variation in the transmitted THz signal amplitude due to the existence of air voids in the CFRP. However, in thicker CFRP, the absorption of THz waves by the carbon fibers is very high, resulting in an undetectable output. Thus, a new technique that is suitable for such an application is required. Therefore, we proposed and developed a reflective THz imaging technology that is able to accurately inspect the sub-surface layer porosity distribution in CFRP, it is a meaningful trying and addition on the existing detection methodology.

2. Modelling

2.1. Principle

CFRP is composed of multiple layers of carbon fibers with epoxy in between, as shown in Fig. 1. It is well known that the existence of air voids in CFRP will change its density and the refractive index too. The variation of the refractive index will lead to a change in the reflectivity of the THz signal based on the Fresnel reflection law. Therefore, we can use the amplitude of the reflected signal to detect the sub-surface layer porosity of CFRP in a reflective THz setup. Furthermore, when air voids exist, the penetration of the THz pulse will be deeper, which will affect the time taken for the reflected THz pulse signal to reach the detector (time of flight, ToF). Thus, we can also use the ToF of the reflected THz signal to detect the sub-surface layer porosity of CFRP in a reflective THz setup.

The refractive index in the transverse electrical (TE) mode when there are air voids in CFRP can be described using effective medium theory (EMT) [18]:

$$n_{CP}^2 = (1 - p)n_{CO}^2 + pn^2, \quad (1)$$

where p is the porosity level, n_{CO} is the refractive index of pore-free CFRP, n_{CP} is the refractive index of CFRP with pores, and n is the refractive index of air, which is a constant of 1. n_{CO} varies from 1.6 to 5 with the ratio of the volumes of carbon and epoxy in CFRP. The refractive index of porous CFRP will be lower than that of pore-free CFRP. The more air voids that exist, the lower the overall refractive index will be, leading to a lower amplitude of reflected THz signals. The more air voids that exist inside the CFRP, the deeper the THz signal will be able to penetrate, and the reflections from different carbon fiber layers will broaden the reflected THz pulse width and lead to a longer ToF before reaching the THz detector.

In the reflection configuration, due to the high loss from the CFRP, the image of the E-field parallel to the carbon fibers mainly shows information about the topmost layers. However, the imaging of the perpendicular E-field can penetrate deeper. This is due to the fact that the absorption is lower when the polarization is perpendicular to the direction of the carbon fibers; thus, the THz beam can go deeper into the material and the inner structures become more visible.

2.2. Reflective THz imaging setup

A diagram of the reflective THz beam penetration in CFRP is shown in Fig. 1. The THz beam is incident and reflected on the sample at an angle of $\theta = 30$ degree. The polarization of the electrical field is perpendicular to the reflection plane. The CFRP sample is illustrated as having a multilayer structure, with each carbon layer and epoxy layer having a refractive index of n_1 and n_2 , respectively. The propagation of THz pulses in media has been extensively studied,[19,20] whereas in this study we are more concerned about air pores in CFRP. The scattering of a coherent THz field can be expressed as [15]:

$$\frac{E_{CFRP}(\omega)}{E_{REF}(\omega)} = EXP\left[\frac{-z}{2l(\omega)}\right] EXP\left[\frac{-\alpha(\omega)z}{2}\right] \frac{4n}{(n+1)^2} \quad (2)$$

where $E_{CFRP}(\omega)$ and $E_{REF}(\omega)$ are the detected THz field with and without the CFRP, respectively, l is the scattering mean free path, α is the absorption coefficient, and z is the thickness of the CFRP. From Eq. (2), the refractive index and absorption coefficient of CFRP can be deduced. A THz-TDS TERA system from Menlo System GmbH, with schematic diagram illustrated in Fig. 2, is used in this study. This system is mode-locked with 150 mW average power, a 100 femto-second ultrashort pulse width, a 1550 nm wavelength fiber laser pump, and a photoconductive switch with a lock-in amplifier. A low-temperature InGaAs-based photoconductive emitter and detector are used to generate and detect THz radiation, respectively. The Menlo THz imaging system can be easily changed into either a transmission or reflective configuration by rotating the emitter and detector on a rail. The TDS system has a maximum scanning frequency range of 150 GHz–3 THz with a maximum dynamic range of ~70 dB under nitrogen purging. The focal length of the THz lens is 100 mm and the full width at half maximum (FWHM) beam width is about 1 mm. By scanning an XY moving stage and obtaining the spectrum by THz-TDS at each pixel, entire images are quickly captured, maximum imaging size are around 5cm×5cm. The Menlo imaging system can automatically output two kinds of THz images, one is based on the THz peak amplitude of the THz pulse in time domain, and the other is based on the ToF from THz emitter to THz detector.

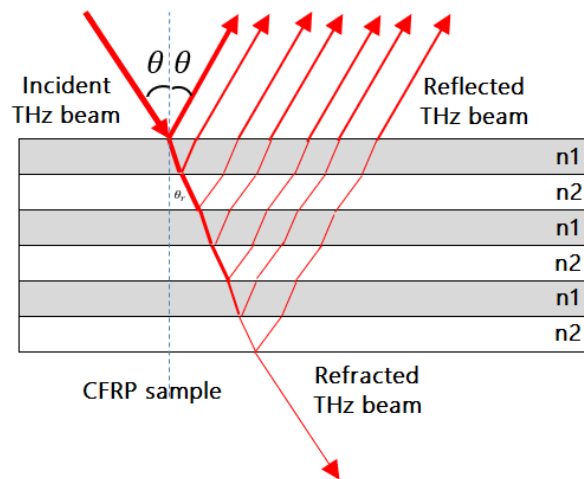


Fig. 1. Penetration of reflective THz beam in CFRP. n1: carbon fiber layer; n2: epoxy (color online)

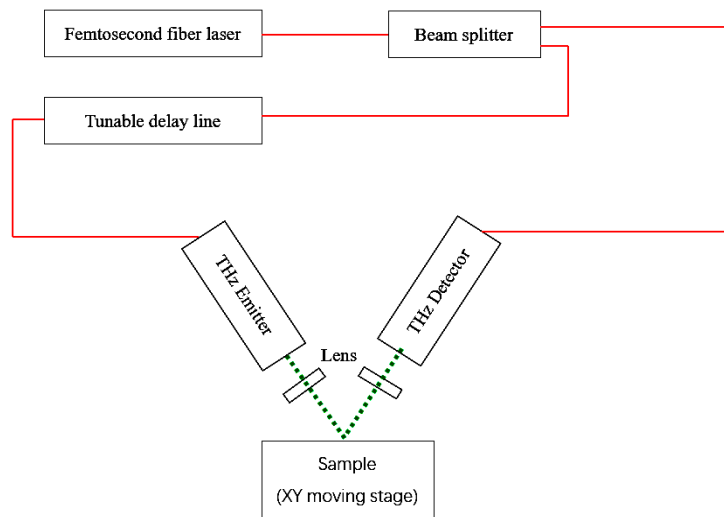


Fig. 2. Diagram of the reflective THz-TDS setup (red solid line: optical fiber; green dot line: THz beam) (color online)

3. Experimental results

3.1. Sample P256-R2

One of the custom-designed and calibrated CFRP samples is a predefined sample P256-R2 by Boeing company, with a matrix layered structure and a total thickness of 1.0 mm, was used for the experiment. The sample had a predefined ring-structure porosity pattern, with the porosity gradually decreasing along the radius. The sample was not sensitive to THz polarization because the carbon fibers were matrix-structured in alternative layers. The right half of the sample was cut and tested with an ionizing X-ray method. Due to its large size, seven zones with different porosities were predefined, as shown in the left of Fig. 3, and the porosity data of those seven zones are listed in Table 1. In the area outside the circle in the figure, the porosity is taken as zero. We used Vernier caliper measured the sample's thickness, the results show the sample has a perfect plane smoothness on the whole sample surface with less than 1 μm variety.

Due to the large size of the sample and the maximum scanning range of our THz-TDS imaging setup, we could only select the area marked by the red square in Fig. 3 left ($\sim 56 \text{ mm} \times 45 \text{ mm}$) for the reflective THz imaging scan, where the step interval of the motor was $\sim 0.13 \text{ mm}$. Fig. 3 shows the acquired THz images of the reflective THz amplitude (top right) and the ToF (bottom right). Here, the THz amplitude is the peak amplitude of the reflected THz pulse in the time domain, whereas the ToF is the flight time of THz pulse from THz emitter to the THz detector and which is defined by pulse peak in the time domain, where both sets of data were obtained by Menlo TERA imaging software. Both results show a ring-structure pattern, which matches the porosity of the original CFRP sample. From this, we can infer that the reflected THz amplitude and the ToF, obtained using the reflective THz-TDS imaging setup, can both be used to non-destructively detect the porosity. It can also be seen that the image of the ToF has a much clearer imaging contrast with better quality than that of the THz amplitude.

Table 1. Porosity measurement data obtained by X-rays

Hot-bonding zone	Zone 1	Zone 2	Zone 3	Zone 4	Zone 5	Zone 6	Zone 7
Porosity (%)	0.15	13	13	11	14	15	2
Standard deviation	0.27	6.4	5.0	4.1	4.7	6.4	2.5

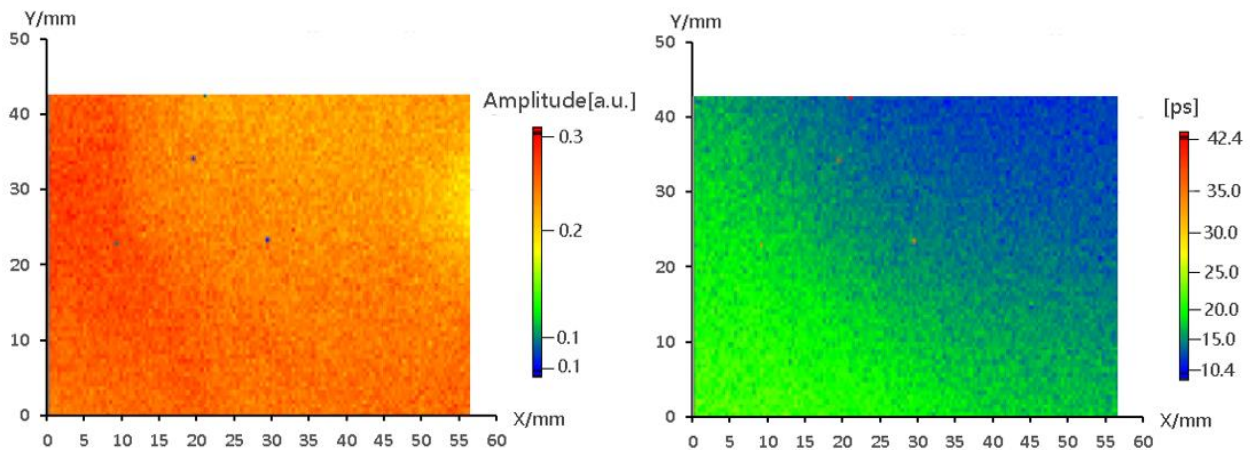
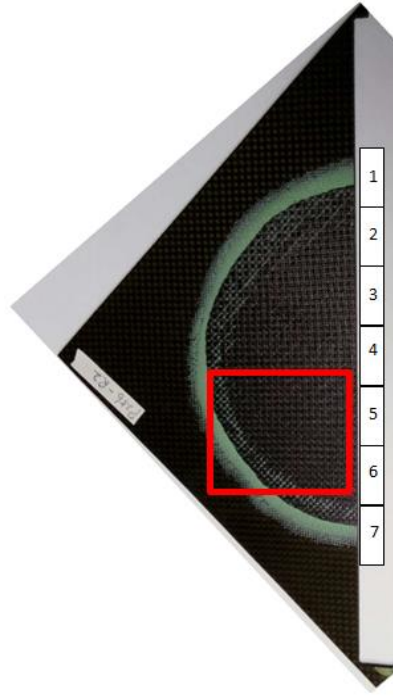


Fig. 3. Top: Photograph of P256-R2 sample and definition of zones. The red square is the THz scanning area. Bottom left: Reflected THz amplitude image. Bottom right: THz image of ToF (color online)

In the time domain, the reflected THz pulse was actually a stretched pulse that was a coherent superposition of all reflections (including Fresnel surface reflection and reflections from all layers and scattering), and the contribution to the pulse shape is smaller from the deeper layers. Frequency domain amplitude signal across wide band have similar imaging results, but with lower signal noise ratio.

3.2. Data analysis

We used the test results of the P256-R2 sample as an example to process data. We tried to correlate the (1) reflective THz peak amplitude, and (2) reflective ToF with the porosity of the sample. We assumed that the surrounding area has a porosity of zero while the center area has the highest porosity value of $\sim 15\%$, which was

tested by ionizing X-rays. The direct output readings of the THz amplitude were 0.28 and 0.07 (a.u.) in the surrounding and center areas, while the output ToFs were 20 and 52 ps in the surrounding and center areas, respectively. We assumed a linear relationship between the porosity and the detected THz parameters, as shown in Fig. 4, and obtained the fitting equations $y = -0.7143x + 0.2$ for the amplitude and $y = 0.0047x - 0.0938$ for the ToF by curve fitting. Using these two equations, we can find the corresponding porosity value through the detected THz data. We also found that there is a maximum detection noise fluctuation of 10% for the raw data for the P256-R2

sample. Hence, we calculated the detection sensitivity of the porosity to be 2.1% and 2.6% for the amplitude test and ToF test, respectively. However, we sometimes found in the experiments that the THz amplitude signal was more easily affected by the sample placement and plane angle alignment. As a result of performing multiple rounds of tests, we estimated the detection sensitivity for our porosity test to be ~3.5% for the amplitude test and ~2.5% for the ToF test, and using both sets of data to evaluate the porosity distribution of a sample will increase the sensitivity.

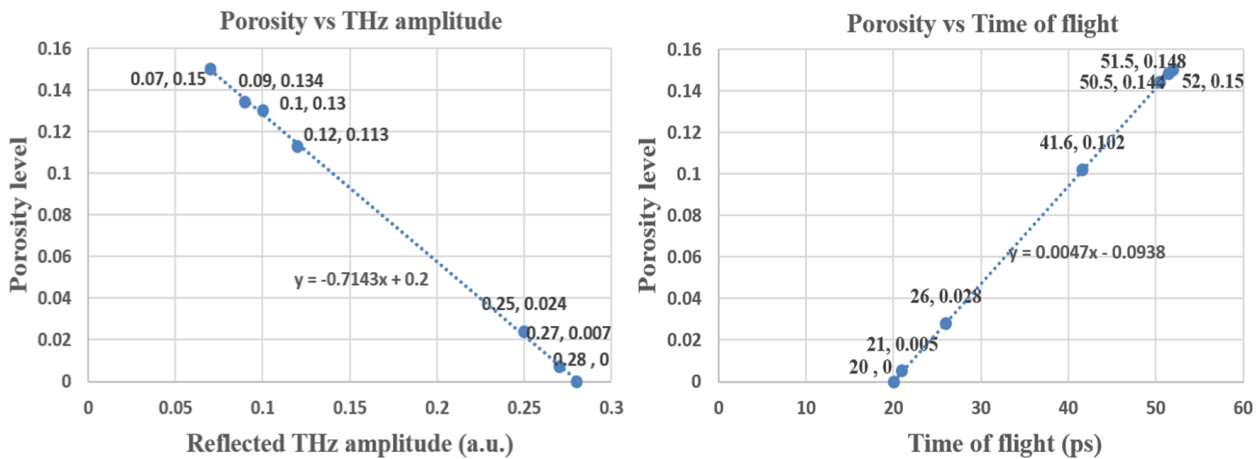


Fig. 4. Porosity level vs detected THz parameters (color online)

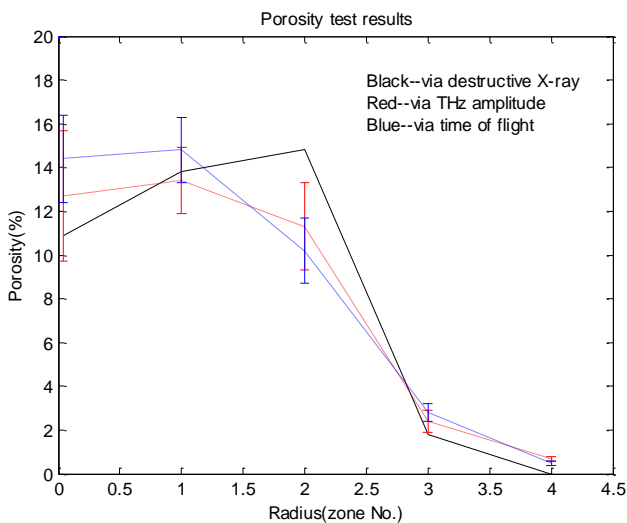


Fig. 5. Porosity test results for P256-R2 sample (color online)

The porosity level in each zone was estimated using the above fitting curves. Fig. 5 shows a comparison of the porosity test results between the X-ray, THz reflective amplitude, and THz ToF methods. The results are in reasonable agreement and show similar trends.

In the experiment, the CFRP surface should be flat to reflect the signal back to the detector. In principle, normal angle incidence and a reflection-based design can further improve the sensitivity of porosity detection, but our THz system can only be adjusted to a minimum incidence angle

of 30° due to the larger emitter/detector size. We also found that such porosity test methods are applicable only to certain depths (top layers with thicknesses of less than 0.5 mm for different CFRPs) due to the loss. A perpendicular E-field can penetrate deeper and provide more information on the internal porosity than a parallel E-field, but this point will be more useful for unidirectional structured CFRP rather than the matrix-structured CFRP considered here. Therefore, the surface roughness variation on the other side of the CFRP will not affect the results in this side tests.

4. Conclusions

Reflective THz imaging is able to detect the sub-surface layer porosity distribution in CFRP. We found that both the reflected peak amplitude of THz pulse in the time domain, and the ToF of reflected THz pulse can be used for non-destructive porosity detection. The sensitivity for our porosity tests was about 3.5 % for the THz amplitude test and about 2.5 % for the ToF test. Both parameters can be used together to evaluate porosity more accurately. Currently, reflective THz imaging can only detect sub-surface layer porosity in the top layers of thick CFRP. Although more research is required to overcome this limitation and improve the detection sensitivity, this THz detection method for CFRP porosity is still a meaningful attempt and shows potential for the NDI of composites in the future. Compared with CFRP, GFRP has

much lower absorption at THz frequencies, thus the above inspection method and algorithms are also valid for GFRP including thick GFRP, and even the latest 3D-printed electronic devices.

Acknowledgements

This work was supported by National Natural Science Foundation of China (Grant No. 62075013) and Key Research Incubation Funding of Beijing Information Science and Technology University (Grant No. 2121YJPY209).

References

- [1] H. Heuer, M. Schulze, M. Pooch, S. Gäbler, A. Nocke, G. Bardl, Ch. Cherif, M. Klein, R. Kupke, R. Vetter, F. Lenz, M. Kliem, C. Bülow, J. Goyvaerts, T. Mayer, S. Petrenz, *Composites Part B: Engineering* **77**, 494 (2015).
- [2] Francisco Maciel Monticeli, Heitor Luiz Ornaghi Jr, Herman Jacobus Cornelis Voorwald, Maria Odila Hilário Cioffi, *Composites Part A: Applied Science and Manufacturing* **125**, 105555 (2019).
- [3] Jie Wang, Jin Zhang, Tianying Chang, Hong Liang Cui, *International Journal of Precision Engineering and Manufacturing* **20**, 963 (2019).
- [4] Franck Ospald, Wissem Zouathi, Rene Beigang, Carsten Matheis, Joachim Jonuscheit, Benoit Recur, Jean-Paul Guillet, Patrick Mounaix, Wouter Vleugels, Pablo Venegas Bosom, Laura Vega Gonzalez, Ion Lopez, Rafael Martinez Edo, Yehuda Sternberg, Marijke Vandewal, *Optical Engineering* **53**(3), 031208 (2013).
- [5] Yandong Gong, Zhuo Zhang, Ke Li, Wenxu Ren, *Microwave and Optical Technology Letters* **63**, 1605 (2021).
- [6] Qiang Wang, Xinyi Li, Tianying Chang, Jin Zhang, Lingyu Liu, Hongbin Zhou, Jinpeng Bai, *Infrared Physics & Technology* **97**, 326 (2019).
- [7] Jin Zhang, Changcheng Shi, Yuting Ma, Xiaohui Han, Wei Li, Tianying Chang, Dongshan Wei, Chunlei Du, Hong-Liang Cui, *Optical Engineering* **54**(5), 054106 (2015).
- [8] Hai Zhang, Henrique C. Fernandes, Ulf Hassler, Clemente Ibarra-Castanedo, Marc Genest, François Robitaille, Simon Joncas, Xavier Maldague, *Optical Engineering* **56**(4), 041304 (2016).
- [9] Jin Zhang, Wei Li, Hong-Liang Cui, Changcheng Shi, Xiaohui Han, Yuting Ma, Jiandong Chen, Tianying Chang, Dongshan Wei, Yumin Zhang, Yufeng Zhou, *Sensors* **16**, 875 (2016).
- [10] Jie Wang, Jin Zhang, Tianying Chang, Lingyu Liu, Hong-Liang Cui, *Infrared Physics & Technology* **98**, 326 (2019).
- [11] Dan-Dan Zhang, Jiao-Jiao Ren, Jian Gu, Li-Juan Li, Ji-Yang Zhang, Wei-Hua Xiong, Yi-Fan Zhong, Tong-Yu Zhou, *Composite Structures* **251**, 112624 (2020).
- [12] Kwang-Hee Im, David Kuei Hsu, Chien-Ping Chiou, Daniel J. Barnard, Sun-Kyu Kim, Sung-Jun Kang, Young-Tae Cho, Jong-An Jung, In-Young Yang, *Materials Science* **20**(4), 457 (2014).
- [13] Xingxing Lu, Huihui Sun, Tianying Chang, Jin Zhang, Hong-Liang Cui, *International Journal of Pharmaceutics* **591**, 120006 (2020).
- [14] Hai Zhang, Stefano Sfarra, Ahmad Osman, Klaus Szielasko, Christopher Stumm, Marc Genest, Xavier P. V. Maldague, *IEEE Transactions on Industrial Informatics* **14**(12), 5629 (2018).
- [15] Liu Hongwei, Ke Lin, *Optics & Laser Technology* **94**(9), 240 (2017).
- [16] Dongdong Ye, Weize Wang, Haiting Zhou, Jibo Huang, Wenchao Wu, Hanhong Gong, Zhen Li, *Optics Express* **27**(2), 28150 (2019).
- [17] Dongdong Ye, Weize Wang, Haiting Zhou, Yuanjun Li, Huanjie Fang, Jibo Huang, Hanhong Gong, Zhen Li, *IEEE Transactions on Terahertz Science and Technology* **10**(4), 383 (2020).
- [18] Banghong Zhang, Yandong Gong, *Optics Express* **23**(10), 14897 (2015).
- [19] P. Jeremy, M. M. Daniel, *Phys. Med. Biol.* **47**(21), 3823 (2002).
- [20] J. R. Fletcher, G. P. Swift, D. C. Dai, J. A. Levitt, J. M. Chamberlain, *J. Appl. Phys.* **101**, 013102 (2007).

*Corresponding author: eydgong@bistu.edu.cn